



LAWRENCE  
LIVERMORE  
NATIONAL  
LABORATORY

# Simultaneous High-Resolution 2-Dimensional Spatial and 1-Dimensional Picosecond Streaked X-ray Pinhole Imaging

A. B. Steel, S. R. Nagel, J. Dunn, H. A. Baldis

May 7, 2012

High-Temperature Plasma Diagnostics  
Monterey, CA, United States  
May 6, 2012 through May 10, 2012

## **Disclaimer**

---

This document was prepared as an account of work sponsored by an agency of the United States government. Neither the United States government nor Lawrence Livermore National Security, LLC, nor any of their employees makes any warranty, expressed or implied, or assumes any legal liability or responsibility for the accuracy, completeness, or usefulness of any information, apparatus, product, or process disclosed, or represents that its use would not infringe privately owned rights. Reference herein to any specific commercial product, process, or service by trade name, trademark, manufacturer, or otherwise does not necessarily constitute or imply its endorsement, recommendation, or favoring by the United States government or Lawrence Livermore National Security, LLC. The views and opinions of authors expressed herein do not necessarily state or reflect those of the United States government or Lawrence Livermore National Security, LLC, and shall not be used for advertising or product endorsement purposes.

# Simultaneous High-Resolution 2-Dimensional Spatial and 1-Dimensional Picosecond Streaked X-ray Pinhole Imaging<sup>a)</sup>

A. B. Steel,<sup>1,2,b)</sup> S. R. Nagel,<sup>1</sup> J. Dunn,<sup>1</sup> and H. A. Baldis<sup>2</sup>

<sup>1</sup>Lawrence Livermore National Laboratory, Livermore, CA 94550, USA

<sup>2</sup>University of California at Davis, Davis, CA 95616, USA

(Presented XXXXX; received XXXXX; accepted XXXXX; published online XXXXX)

A Kentech x-ray streak camera was run at the LLNL Compact Multipulse Terawatt (COMET) laser to record simultaneous space- and time-resolved measurements of picosecond laser-produced plasmas. Four different x-ray energy channels were monitored using broad-band filters to record the time history of Cu targets heated at irradiances of  $10^{16}$  -  $10^{19}$  W/cm<sup>2</sup>. Through the Cu filter channel, a time-resolution below 3ps was obtained. Additionally, an array of 10  $\mu\text{m}$  diameter pinholes was placed in front of the camera to produce multiple time-resolved x-ray images on the photocathode and time-integrated images on the phosphor with 10 and 15 times magnification, respectively, with spatial resolution of  $<13 \mu\text{m}$ .

## I. INTRODUCTION

X-ray streak cameras have been utilized for decades to view events that occur on increasingly short time scales, with modern ultrafast streak cameras being able to record light phenomena with sub-picosecond time resolution<sup>1,2,3,4,5</sup>. Streak cameras provide intensity vs. time and one spatial dimension. It's also been shown that 2-D time-resolved pinhole images could be generated using a pinhole array that is rotated by a small angle from the streak camera entry slit<sup>6,7</sup>. Here, we calibrate the temporal and spatial resolution of a Kentech streak camera that utilizes a pinhole array to achieve a 2-D time-integrated image as well as a streaked pinhole image. The time-integrated images had a spatial resolution of  $<13 \mu\text{m}$  and the time-resolved streaked images indicate a temporal resolution better than 3 ps.

## II. EXPERIMENTAL SET-UP

The experiment was performed on the COMET<sup>8</sup> laser at the LLNL Jupiter Laser Facility (JLF). We employed a single 1053 nm beam with pulse durations of 500 fs and 5 ps with energies of 5 – 10 J to produce irradiances ranging from  $10^{16}$  -  $10^{19}$  W/cm<sup>2</sup> on a Cu target. The X-ray Streak Camera (XRSC) fielded was a commercially available Low Magnification Kentech Instruments model. A 250  $\mu\text{m}$  entry slit was used with two photocathode set-ups: a 306  $\text{\AA}$  Au/1025  $\text{\AA}$  Lexan (C<sub>16</sub>H<sub>14</sub>O<sub>3</sub>) photocathode was used with a 3 mm photocathode/mesh spacer, and a 1239  $\text{\AA}$  CsI/242  $\text{\AA}$  Au/949  $\text{\AA}$  Lexan photocathode with a 1 mm spacer. The XRSC was coupled to a 40mm diameter Photek MCP image intensifier and a 4096  $\times$  4096 pixel array CCD camera made by Spectral Instruments. The CCD pixels measured 9  $\mu\text{m}$   $\times$  9  $\mu\text{m}$ . The XRSC was operated on the fastest sweep speed and viewed targets at a shallow angle through four different broad-band filters. These filter channels included a light-tight filter of 1  $\mu\text{m}$  polypropylene (C<sub>3</sub>H<sub>6</sub>)/342 nm Al followed by either: 2  $\mu\text{m}$  Cu/2  $\mu\text{m}$  polypropylene, 6  $\mu\text{m}$  Al, 8  $\mu\text{m}$  Kapton (C<sub>22</sub>H<sub>10</sub>N<sub>2</sub>O<sub>5</sub>)/244 nm Al, 100  $\mu\text{m}$  Al straight-through block, or no additional filtering.

<sup>a)</sup>Contributed paper published as part of the Proceedings of the 19th Topical Conference on High-Temperature Plasma Diagnostics, Monterey, California, May, 2012.

<sup>b)</sup>Author to whom correspondence should be addressed: steel1@llnl.gov.

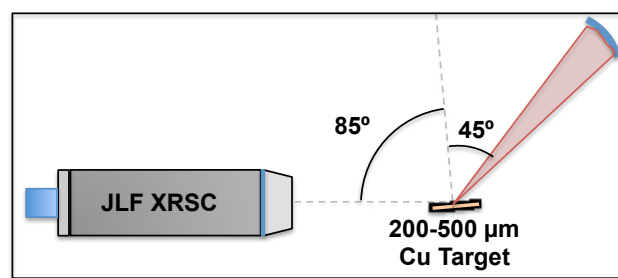


Figure 1: Experimental set-up.

## III. RESULTS

### A. SWEEP SPEED CALCULATION

When the CsI photocathode was used, an array of 250  $\mu\text{m}$  horizontal slits was placed directly in front of the photocathode slit. This created several streaked lines on the CCD who's lineouts, along with the electrons' drift velocity, were used to calculate the camera's sweep speed. The drift velocity was determined by calculating the field strengths within the XRSC based on the given electric potentials. A final drift velocity of  $0.177 \pm 0.005$  mm/ps was obtained for x-rays incident on the center of the photocathode. The error comes from the uncertainties in the positions of the photocathode, mesh, electron optics, and anode.

The x-rays incident on the top and bottom of the photocathode produce electrons that must travel farther than those at the center because the electron optics in the XRSC focus the electrons through a hole in the anode. This added flight time is calculated from the electron's drift velocity and creates a parabolic contour on the CCD (Figure 2). Each point on a contour arrived at the photocathode at the same time, but arrived at the CCD at different times based on its special position.

The added flight time along with the change in the position of the peak emission time on the time axis as a function of its position on the spatial axis was then used to determine the sweep speed, which for the shot in Figure 2 was determined to be  $4.4 \pm$

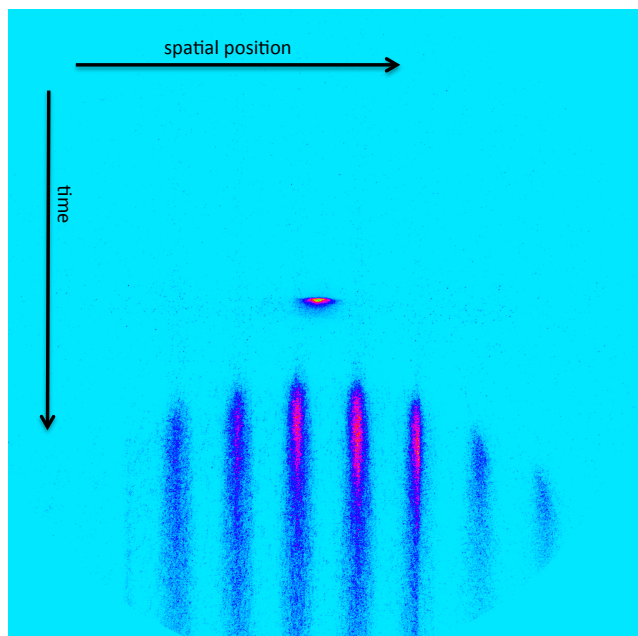


**Figure 2:** (Colour Online) Pinhole shot. The center spot is a time-integrated image. The time-resolved images are streaked below, showing the parabolic contours.

0.7 ps/mm. Here the uncertainty is a combination of the contour fit parameters and the uncertainty in the drift velocity. Several of these fits were generated for sweeps starting at varying positions on the time axis. This allowed us to view how the sweep speed changes as a function of its position in time (see figure 3). We found that the sweep speed was not constant across the time window, and was actually getting faster as it moved forward in time. This is believed to be caused by some non-linearity in the ramp voltage.

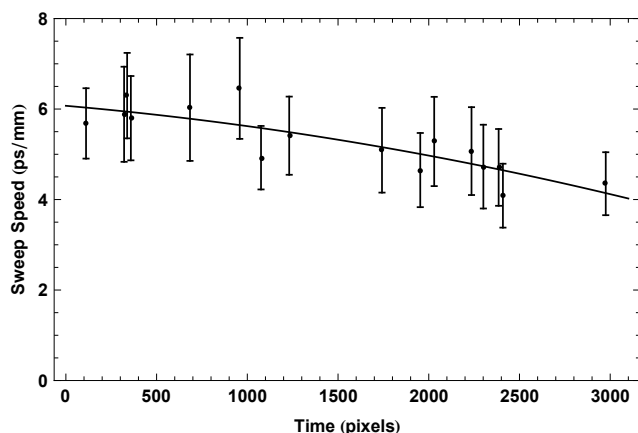


**Figure 3:** This graph shows the sweep speed versus position on the time axis. The fit was weighted with the errors for each sweep speed calculation to produce a better overall fit.

## B. X-ray Temporal Measurements

The x-ray emission from the laser heated Cu target showed different time signatures. The softer filtered energy channels lasted longer than the harder filtered channels by several picoseconds. The Cu filtered channel had the shortest time

history by filtering out the thermal x-ray emission below 2keV and allowing only the hard x-ray continuum and K $\alpha$  x-rays to pass through. The CsI coated photocathode was used primarily to increase the signal level in the Cu filtered energy band. This is achieved by increasing the secondary electron production.<sup>9,10</sup> The horizontal slit array that was added in front of the photocathode slit reduced the temporal broadening space-charge effects<sup>11</sup> present in the streak camera.

A magnification of  $1.16 \pm 0.02$  was measured due to electron optics in the XRSC. With a photocathode slit of 250  $\mu\text{m}$ , the best temporal resolution was limited to between  $1.24 \pm 0.04$  and  $1.74 \pm 0.03$  ps, depending on the sweep window.

Data from both the CsI and Au photocathode were analyzed. Data with low signal-to-noise or space-charge distortion were removed from analysis.

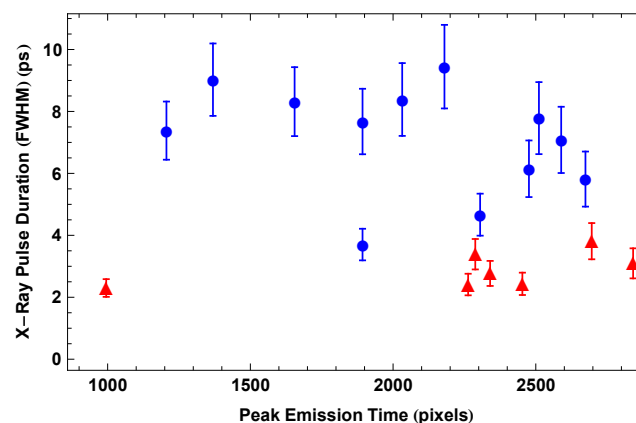


**Figure 4:** (Colour Online) The red triangles are for a 500 fs laser pulse and a CsI coated photocathode. X-ray emission of fewer than 5 ps was consistently measured. The blue circles had a 5 ps pulse and a Au photocathode. Here the x-ray emission was still below 10 ps for most shots.

Laser pulse lengths of 500 fs were found to produce very short x-ray emission that, on average, was  $2.9 \pm 0.4$  ps in duration (FWHM). With the Au photocathode in place, 5 ps laser pulses were observed to produce x-ray emission with an average duration of  $8 \pm 1$  ps. However, by deconvolving the geometry of the streak camera's electron optics, lineouts could be added together for the same shot to increase the statistics. By employing this method, x-ray emission of  $7 \pm 1$  ps was measured (Figure 4). The uncertainty in measured x-ray emission occurs from the error in the sweep speed. A minimum x-ray emission duration time of  $2.3 \pm 0.3$  ps was recorded. It can therefore be determined that the temporal resolution of the XRSC is on the order of 2 ps.

## C. Pinhole Imaging

An array of 10  $\mu\text{m}$  diameter pinholes on a 100  $\mu\text{m}$  Ta substrate was added in front of the streak camera entry slit (Figure 5). When using the pinhole array, the entry slit to the photocathode was replaced. The larger 760  $\mu\text{m}$  slit ensured only one row of pinholes would illuminate the photocathode, and thus the spatial resolution is determined by a virtual photocathode slit created by the pinhole size and not the actual photocathode slit width. X-rays streaming through the photocathode and directly illuminating the phosphor created a 2-D time-integrated image. The magnification of such images is  $\sim 15.3$  with an estimated spatial resolution of 10.65  $\mu\text{m}$ . Radiation that is converted into

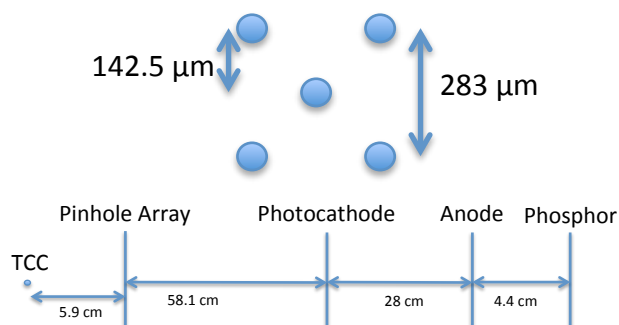


**Figure 5:** The arrangement of the pinholes on the array is shown above. Each of the approximately 100 pinholes measures  $\sim 10 \mu\text{m}$  in diameter. Below is the relative location for each element responsible for the magnification of the pinhole images.

photoelectrons at the cathode undergo a magnification of  $\sim 9.8$ , then get magnified once more by the electron optics for a total magnification of  $\sim 11.4$  with an estimated spatial resolution of  $10.88 \mu\text{m}$ . The fluence of hard x-rays through the pinhole was low and did not produce a useable image in the Cu filtered channel.

When using the pinhole array, it was discovered that the target was not actually sitting at the best focus of the focusing parabola. Figure 6 shows how the focal spot size changed in the height direction as a function of the change in the targets position from what was out nominal best focus.

The streaked time-resolved pinhole images also gave measurements for the focal spot size. In general, these spot sizes (which were taken during the peak emission time) were smaller than the time-integrated spot sizes. There were also far fewer of them to measure as the signal-to-noise ratio was often too low to get good statistics. As shown by the red circles on Figure 6, there are three different groups of spot sizes. A spot size of over  $100 \mu\text{m}$  corresponds to a z position that was less than the best focus. A spot size between  $70$  and  $90 \mu\text{m}$  occurred at a wide spread of z positions and seemed to be more dependent on the height on the target. Spot sizes that were less than  $60 \mu\text{m}$  only happened with a z position of  $+150 \mu\text{m}$  or better from best focus. The only time the spot size was less than  $60 \mu\text{m}$  was in the few shots immediately after starting a new column on the target. The importance of the height shot on the target for all spot sizes less than  $100 \mu\text{m}$  implies that the target was either not aligned perpendicular to the focal axis of the laser, or was warping. Upon inspection of the targets after they were removed from the target chamber, it was noticed that the targets were indeed warping. This could have been remedied by using either thicker Cu, or by mounting the target on a substrate.

The blue squares in Figure 6 show measurements of the same time-integrated pinhole images as the red data, but taken in the direction normal to the target, where the plasma blows off. These lineouts all had a FWHM of less than  $20 \mu\text{m}$ , with an average of  $\sim 13 \mu\text{m}$ . Extrapolating this to the photocathode, a virtual slit of  $\sim 150 \mu\text{m}$  was produced by using the pinhole array.

## IV. DISCUSSION

The sweep speed and temporal resolution were calibrated for the fastest sweep speed of a standard Kentech XRSC. A sweep speed ranging from  $6 \pm 0.3$  to  $4 \pm 0.7$  ps/mm was measured depending on the position within the sweep window. A minimum x-ray emission time of  $2.3 \pm 0.3$  ps was recorded for a laser pulse of  $500$  fs by looking through a Cu filter, suggesting a temporal resolution of approximately  $2$  ps.

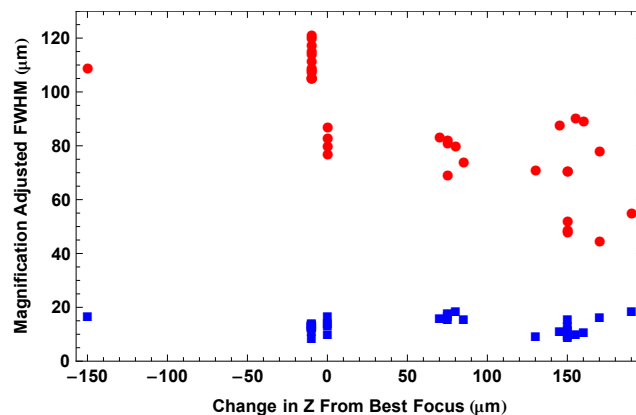


**Figure 6:** (Colour Online) The red circles show the FWHM of the time-integrated pinhole image in the height direction. The blue squares are the FWHM of the time-integrated pinhole images in the blowoff direction.

Using a  $10 \mu\text{m}$  diameter pinhole array, spatial features smaller than  $13 \mu\text{m}$  were measured. This agrees nicely with the estimated spatial resolution of just under  $11 \mu\text{m}$ .

## XII. ACKNOWLEDGEMENTS

This work performed under the auspices of the U.S. Department of Energy by Lawrence Livermore National Laboratory under Contract DE-AC52-07NA27344.

<sup>1</sup>G.L. Stradling, D.T. Attwood, and R.L. Kauffman, *J. Quant. Elec.* **19**, 604 (1983).

<sup>2</sup>M.M. Murnane, H.C. Kapteyn, and R.W. Falcone, *Appl. Phys. Lett.* **56**, 20 (1990).

<sup>3</sup>R. Shepherd, R. Booth, D. Price, M. Bowers, D. Swan, J. Bonlie, B. Young, J. Dunn, B. White, and R. Stewart, *Rev. Sci. Instrum.* **66**, 719-721 (1995).

<sup>4</sup>P. Audebert, R. Shepherd, K.B. Fournier, O. Peyrusse, D. Price, R. Lee, P. Springer, J.-C. Gauthier, and L. Klein, *Phys. Rev. Lett.* **89**, 265001 (2002).

<sup>5</sup>D.J. Hoarty, S.F. James, C.R.D Brown, B.M. Williams, T. Guymer, M. Hill, J. Morton, D. Chapman, R. Shepherd, J. Dunn, G. Brown, M. Schneider, P. Beiersdorfer, H.K. Chung, J.W.O. Harris, L. Upcraft, C.C. Smith, and R.W. Lee, *J. Phys.: Conf. Ser.* **244**, 012002 (2010).

<sup>6</sup>O. L. Landen, *Rev. Sci. Instrum.* **63**, 5078 (1992).

<sup>7</sup>H. Nishimura, M. Tanabe, T. Fujiwara, S. Fujioka, H. Shiraga, and H. Azechi, *J. Phys.: Conf. Ser.* **244**, 032056 (2010).

<sup>8</sup>J. Dunn, J. Nilsen, A.L. Osterheld, Y. Li, and V. N. Shlyaptshev, *Opt. Lett.* **24**, 101-103 (1999)

<sup>9</sup>G.L. Stradling, H. Meddecki, R.L. Kauffman, D.T. Attwood, and B.L. Kenke, *Appl. Phys. Lett.* **37**, 782 (1980).

<sup>10</sup>B. L. Henke, J.P. Knauer, and K. Premaratne, *J. Appl. Phys.* **52**, 1509 (1981).

<sup>11</sup>B. Qian and H. Elsayed-Ali, *J. Appl. Phys.* **91**, 462 (2002).